Science of the Total Environment 630 (2018) 1057–1070

Contents lists available at ScienceDirect

Science of the Total Environment

journal homepage: www.elsevier.com/locate/scitotenv

An observational study of nitrous acid (HONO) in Shanghai, China: The aerosol impact on HONO formation during the haze episodes

Lulu Cui [a], Rui Li [a], Yunchen Zhang [a], Ya Meng [a], Hongbo Fu [a,b,c,*], Jianmin Chen [a,**]

[a] Shanghai Key Laboratory of Atmospheric Particle Pollution and Prevention, Department of Environmental Science & Engineering, Institute of Atmospheric Sciences, Fudan University, Shanghai 200433, China
[b] Shanghai Institute of Pollution Control and Ecological Security, Shanghai 200092, China
[c] Collaborative Innovation Center of Atmospheric Environment and Equipment Technology (CICAEET), Nanjing University of Information Science and Technology, Nanjing 210044, China

HIGHLIGHTS

- HONO showed a higher level during the haze/fog period.
- The heterogeneous conversion of NO_2 to HONO was prompted during the haze/fog period.
- Aerosol surface played a role in heterogeneous NO_2 conversion.
- S/N-bearing particles showed a relative higher proportion during the pollution period.

GRAPHICAL ABSTRACT

This figure represents the correlations between $HONO_{correct}/NO_2$ and RH and $PM_{2.5}$ concentration at night, respectively.

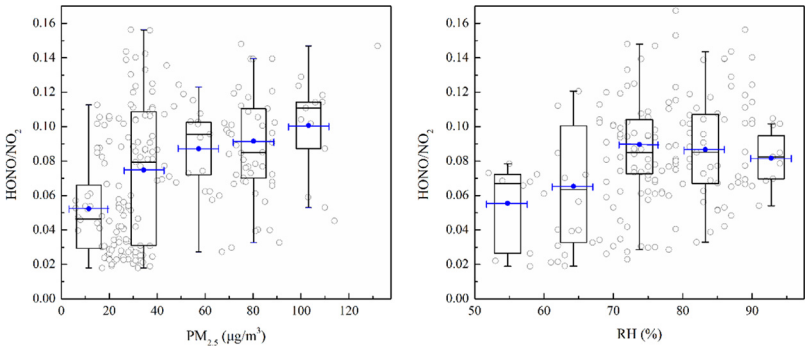

ARTICLE INFO

Article history:
Received 19 December 2017
Received in revised form 31 January 2018
Accepted 6 February 2018
Available online xxxx

Editor: Jay Gan

Keywords:
Air quality
HONO
NO_2
Aerosol
Haze episode
China

ABSTRACT

Continuous HONO measurement was conducted to study the formation features of HONO during the haze episodes at Shanghai, China. The HONO concentration ranged from 0.26 to 5.84 ppb and averaged at 2.31 ppb during the measurement period. The HONO concentration during the haze episode (P1), the haze-fog episode (P2) and the clean period (P3) were 2.80, 2.35 and 1.78 ppb, respectively. Heterogeneous conversion of NO_2 was the dominate pathway for nocturnal HONO formation, and the heterogeneous conversion efficiency of NO_2 to HONO was closely associated with the $PM_{2.5}$ concentration. The averaged heterogeneous conversion rate of NO_2-to-HONO (C_{HONO}) during the pollution periods (P1 + P2) was 1.58×10^{-2} h^{-1}, higher than that during the clean period (P3) (0.93×10^{-2} h^{-1}), suggesting the higher conversion potential of NO_2 to HONO during the pollution episodes. The daytime unknown HONO production rate ($P_{unknown}$) in the pollution period was 2.98 ppb/h, higher than 1.78 ppb/h in the clean period. Further, aerosol played a role in $P_{unknown}$ during the transformation of the clean period to the pollution period. At a single particle scale, transmission electron microscopy (TEM) images revealed that most of the particles during P1 and P2 were agglomerated, whereas the particles collected from P3 were uniformly distributed and showed simple morphologies. The number percentage of the S/N-bearing particles during P1 (34%) and P2 (27%) were higher than that during P3 (20%). In addition, particles contained more internally mixed nitrates during P1 and P2 than those during P3, suggesting more intense heterogeneous conversion of NO_2 to HONO on particle surfaces during the pollution episodes. In the present study, the averaged HONO/

* Correspondence to: H. Fu, Shanghai Key Laboratory of Atmospheric Particle Pollution and Prevention, Department of Environmental Science & Engineering, Institute of Atmospheric Sciences, Fudan University, Shanghai 200433, China.
** Corresponding author.
E-mail addresses: fuhb@fudan.edu.cn (H. Fu), jmchen@fudan.edu.cn (J. Chen).

https://doi.org/10.1016/j.scitotenv.2018.02.063
0048-9697/

NO_x ratio (5.60%), especially during P1 (7.80%) and P2 (7.50%) was much higher than that assumed global averaged value of 2.0%, suggesting a potentially important role for the HONO chemistry in Shanghai. This study provides new insights into the HONO formation mechanism in the atmosphere characterized by high fine particle level.

1. Introduction

HONO plays an important role in tropospheric photochemistry due to its photolytic production of hydroxyl radical (OH), which governs the oxidizing capacity of the atmosphere and promotes the formation of secondary aerosols in the urban atmospheres (Sörgel et al., 2011). It is well known that HONO accumulates at night, and serves as a primary OH source in the first 2–3 h after sunrise when OH radicals yielded from photolysis of ozone and formaldehyde is relatively low (Czader et al., 2012). Filed measurements and modeling studies revealed that on average up to 25–50% of the daily OH budget in the troposphere was derived from the HONO photolysis (Sörgel et al., 2011; Acker et al., 2006; Su et al., 2008; Kleffmann et al., 2005). Hendrick et al. (2014) have reported that the contribution of the HONO photolysis to OH budget could reach up to 90% around 12:00–13:00 in the Beijing winter. OH initiates most oxidation reactions in the atmosphere, i.e., it can oxidize SO_2 and NO_2 to H_2SO_4 and HNO_3, respectively, which could be further condensed on aerosol surfaces to form sulfates and nitrates (Zhou et al., 2013). Elevated concentrations of NO_3^- and SO_4^{2-} together with their hygroscopic growth could cause visibility impairment and enhance the incidence of regional haze under stagnant weather conditions (An et al., 2013). In addition, OH radical can react with VOCs to form secondary aerosols, which could serve as cloud nuclei (CCN, Duplissy et al., 2008). In this way HONO exerts an indirect effect on regional and/or global climate.

HONO in the atmosphere was assumed to be in a pseudo steady state (PSS) during daytime, which was balanced by the reaction of nitric oxide (NO) and OH in the gas phase, and the losses via its photolysis and/or the reaction with OH (Kleffmann et al., 2005; Villena et al., 2011). However, obvious discrepancies were found between simulated HONO values calculated from PSS and observed HONO concentrations during both daytime and nighttime, even considering the direct emission (Kleffmann et al., 2005; Kurtenbach et al., 2001; Stutz et al., 2004; Sörgel et al., 2011). Heterogeneous processes on aerosol surfaces have been proposed as an explanation for the missing HONO sources (Li et al., 2012; Liu et al., 2014; Huang et al., 2017). The hydrolysis and redox reaction of NO_2 has been extensively investigated on various aerosol surfaces including soot, minerals and organic-coated surfaces (Ammann et al., 1998; Aubin and Abbatt, 2007; Kleffmann et al., 1999). Minerals and transition metals could effectively catalyze the hydrolysis reaction of NO_2 adsorbed on surfaces (Zhou et al., 2015; Grassian, 2002; Wang et al., 2003). Besides, the photosensitized conversion of NO_2 on organic surfaces has been proposed as an effective pathway to generate HONO (Han et al., 2016; Ammann et al., 1998; Kleffmann et al., 1999; Stemmler et al., 2006). The conversion efficiency of NO_2 to HONO depends not only on theNO_2 concentration, but also on the absorbed moisture content and surface area (Finlayson-Pitts et al., 2003). Studies conducted in the urban regions already reveal a good correlation between the PM concentration and the HONO level, or between specific surface area of the particles and the HONO concentration (An et al., 2009; Ziemba et al., 2010). An et al. (2011) reported that the heterogeneous conversion of NO_2 on aerosol surfaces could contribute to 59% of the ambient HONO in Jing-Jin-Ji area, which was primarily attributed to high concentration of particulate matter (PM). These findings suggest that aerosol surfaces might play a significant role in HONO production in the atmosphere characterized by high aerosol loads."

Due to rapid economic development and urbanization, haze and fog events characterized by high level of fine particulate matter ($PM_{2.5}$) and low visibility have occurred during the past decades in China, especially in the most developed and densely populated cities (Chan and Yao, 2008; Fu and Chen, 2017; Guo et al., 2014; Huang et al., 2014; Zhang et al., 2013). It was well documented that secondary sulfates and nitrates within the particles deriving from the heterogeneous transformation of NO_2 and SO_2 are effective factors for visibility impairment (TenBrink et al., 1996; Kim et al., 2008). As one of the main products of the heterogeneous NO_2 conversion on aerosol surfaces, the HONO level in the atmosphere is expected to be higher during the haze period as compared to the clean period. The surface area density and chemical nature of aerosol particles are the two dominate factors that control the conversion efficiency of NO_2 to HONO. However, due to the large abundance and complex composition of aerosols, the aerosol surface still provides a poorly understood media for heterogeneous HONO formation (Pathak et al., 2009; Taketani et al., 2012). Various "bulk" techniques (e.g., MARGA, High-resolution time-of-flight aerosol mass spectrometry, Twin Differential Mobility Particle Sizer) were used to determine the chemical compositions and surface area density of particles (Hu et al., 2016; Li et al., 2012; Sun et al., 2010). However, these techniques could not provide details of the actual mixing state of individual particles in the atmosphere. Individual particle analysis by TEM has become a reliable technique to examine the morphology, composition, and mixing state of particles (Li et al., 2013; Li and Shao, 2009; Zhang et al., 2013). This kind of detailed information about individual particles is critical to evaluate their formation, sources and hygroscopic properties, as well as to explain atmospheric processes occurred on particle surfaces. As the largest metropolis in China, Shanghai has a population of approximately 24 million by the year 2013 (Han et al., 2017). Due to rapid economic development and urbanization, Shanghai is suffering from severe haze pollutions (Feng et al., 2009; Hu et al., 2016; Ye et al., 2003). Up to date, the formation features of HONO from airborne sources during the haze/fog episodes have been rarely studied in Shanghai. In the present study, a continuous HONO measurement was performed during a pollution episode in Shanghai using a long path absorption photometer (LOPAP) equipment. Aerosol particles were also collected during the measurement period. The morphologies and chemical compositions of individual particles were characterized using TEM-EDX. Single particle types during different weather types were classified. The hygroscopic behavior of aerosols and the atmospheric heterogeneous processes relating to HONO formation on aerosol surfaces were discussed. The data shown herein will cast a light on the influence of aerosol on the HONO generation in the pollution atmosphere.

2. Experimental section

2.1. The measurement site

The measurement was conducted on the rooftop of a five-storey teaching building on the campus of Fudan University in Yangpu district of Shanghai (Fig. S1). The measurement site is about 20 m above the ground. It is surrounded by residential and commercial districts, and there are no high buildings around within 100 m. Central Ring Road with heavy traffic loading is located south of the site (about 150 m away) and Wudong Road with light traffic is located north of (about 120 m away) the site. National Container Processing Company and Baosteel factory are located at the north of the site with distances of about 15 km and 21 km, respectively. Two waste incineration facilities

named Yuqiao and Jiangqiao, are located at nearly 16 km to the south and 13 km to the west of the site, respectively. Wujing Power Plant and Waigaoqiao No. 3 Power Plant are located to the south and east of the site with distances of about 12 km and 13 km, respectively (Hu et al., 2016). The site could be regarded as a representative urban area under the comprehensive influence of traffic, residential, industrial and construction sources, but not dominated by any of these sources (Fu et al., 2012).

2.2. Measurement instruments

2.2.1. HONO measurement

The measurement of HONO was conducted from 12 May to 28 May 2016 using a commercial LOPAP instrument (QUMA, Model LOPAP-03, QUMA Elektronik & Analytik, Wuppertal, Germany). LOPAP is a wet-chemical in situ measuring instrument with which ambient HONO is sampled as nitrate using absorption solution (R1, a mixture of 100 g sulphanilamide and 1 L 37 wt% hydrochloric acid in 9 L of pure water) in two temperature-controlled stripping coils in series. In the first coil, almost all of HONO and any known interfering species (e.g. NO_2, SO_2 and phenols) were absorbed in the first stripping coil, leaving only the fraction of interfering substances in the second stripping coil. The absorption solution from two coils was then pumped by a peristaltic pump to react with a dye solution (R2, 0.8 g *n*-(1-naphtyl)-ethylendiamine-dihydrchloride in 8 L of pure water) to form a stable diazonium salt, which was subsequently detected photo-metrically using the long-path absorption in a 2.5 m long Teflon tubing. The interference-free HONO concentration was determined from the difference between the signals in the two channels. The operating conditions performed for the LOPAP system have the advantage that HONO was completely sampled even at low pH (Zellweger et al., 1999; Genfa et al., 2003). Additionally, several chemical interferences caused by NO_2 and SO_2 (Spindler et al., 2003) or phenols (Ammann et al., 2005) could be minimized at low pH (Heland et al., 2001; Kleffmann et al., 2002).

During the operation of the instrument, the calibration was performed using 0.01 mg/L nitrite standard solution every week. To correct for the small drifts in the baseline of the instrument, regular automatic zero measurements were performed every 12 h by introducing synthetic air at a flow rate of 1 L/min. Before the campaign, the sampling efficiency of HONO in the sampling unit was determined using a pure HONO-source, and was found to be 99.96%. The instrument has a detection limit of 3.9 ppt for a response time of 4.17 min. The precision and accuracy of the instrument are 1% and 7%, respectively, based on the uncertainties of gas and liquid flow, concentration of calibration standard solution and regression of calibration.

2.2.2. Measurements of trace gases, particles and meteorological parameters

The concentrations of NO, NO_2, and NO_x were measured by nitrogen oxides analyzer (Thermo 42i, Thermo Fisher, USA) with the detection limit of 1.0 ppbv. O_3 was measured by a UV photometric analyzer (Thermo 49i, Thermo Fisher, USA) based on ultraviolet absorption method with a detection limit of 0.5 ppbv. SO_2 was measured by a pulsed fluorescence analyzer (Thermo 43i, Thermo Fisher, USA) with a detection limit of 0.5 ppbv. A gas filter correlation analyzer with the lowest detection limit of below 1 ppmv was used to measure the CO concentration. $PM_{2.5}$ concentration was measured using a Handheld DustTrak DRX Aerosol Monitor (TSI Model 8534, Shoreview, America). The DustTrak measures particles with a size range of 0.1–15 μm at the concentration scope of 0.001–150 mg/m^3, and the detection limit of the instrument is 0.01 μg/m^3 (Li et al., 2015). The instrument was wiped with isopropyl alcohol approximately every 24 h. The meteorological data including wind speed (WS), wind direction (WD), relative humidity (RH) were measured by automatic weather monitoring system (HydroMetTM, Vaisala). Atmospheric visibility was measured by a visibility sensor (Belfort, Model 6000). Calibration of the sensor was performed using the 90001 Calibration Kit recommended by the manufacturer (Visibility Sensor Maunal, Belfort Instrument Company). The screened original data of WS, WD, RH and visibility were averaged to a time resolution of 1 h. All the meteorological data and atmospheric visibility were available on the website https://www.aqistudy.cn/.

2.2.3. Single particle analysis

Aerosol particles were collected using a single-stage cascade impactor with a 1.0-mm-diamater jet nozzle onto the copper grids with

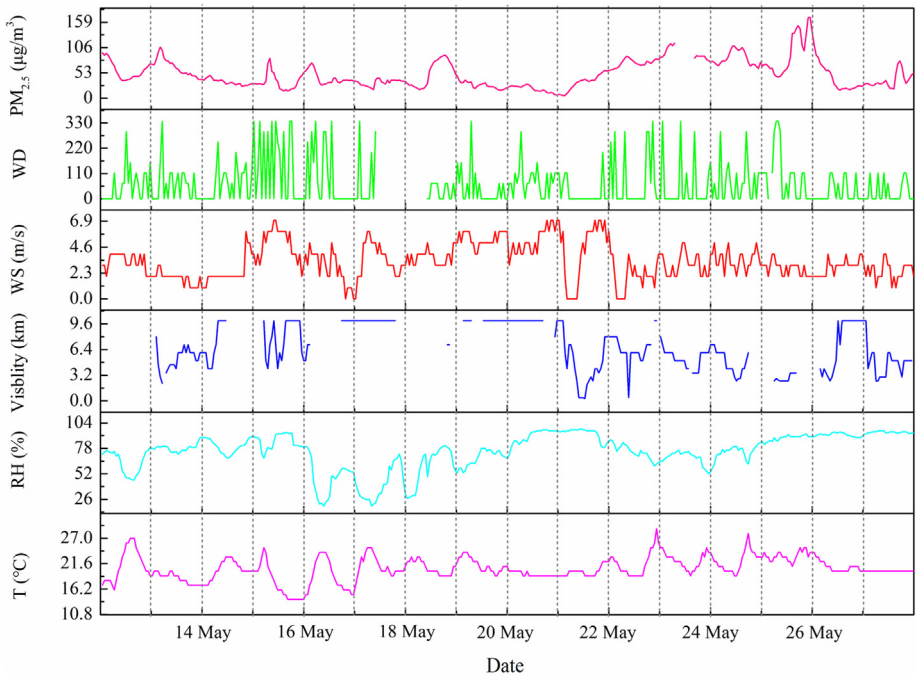

Fig. 1. Time series of the $PM_{2.5}$ concentration and the meteorological parameters (WS, WD, RH, T, visibility).

Table 1
Classification of the meteorological data and the corresponding $PM_{2.5}$ concentration during the measurement period.

Time period	Weather division	$PM_{2.5}$ (μg/m^3)	Temperature (°C)	Relative humidity (%)	Averaged wind speed (m/s)
Haze (P1)	12 May, 16 May, 23 May, 24 May	18–169	15–26	19–80	2.9
Haze-fog (P2)	13 May, 14 May, 15 May, 22 May, 25 May, 28 May	7–138	14–28	62–96	3.2
Clean (P3)	17 May, 19 May, 20 May	7–82	15–26	22–94	4.2
Haze and raining	21 May, 26 May, 27 May	7–110	19–25	86–97	3.2

carbon films (Bu et al., 2015). The collection efficiency of the sampler is 100% at 0.5 μm aerodynamic diameter for particle density of 2 g/cm^3 (Fu et al., 2012). The sampling duration varied between 1 and 20 min according to the particle loading. The collected samples were preserved in a sealed dry plastic carrier, and then stored in a desiccator to avoid contamination.

Particles morphologies and mixing states were analyzed with a 200-kV FEI Tecnai F20 field emission high-resolution transmission electron microscope (FE-HRTEM) (Hu et al., 2016). As particles on the grids were not uniformly distributed, three to four areas were selected from the center to the periphery in a line on each grid to ensure that the analyzed particles were more representative of the entire size range (Hu et al., 2015). Elemental composition were analyzed semiquantitatively by an Oxford energy-dispersive X-ray spectrometer (EDS) that detect elements heavier than carbon. As the TEM grids were made of copper and carbon, Cu and C were ruled out from the analysis. To minimize the beam damage to sensitive particles, exposure time of 15 s was chosen for EDS analysis. The structures of crystalline particles were examined by selected area electron diffraction (SAED) patterns or HRTEM images (Li et al., 2011).

The mass fraction for an element X P(X) in an individual particle was used as an indicator to distinguish the particle compositions (Okada et al., 2005). $P(X) = X / (N + F + Na + Mg + Al + Si + S + Cl + K + Ca + Mn + Fe + Cr + Zn + Pb + Ti + V)$. The particles featured with the highest mass fraction of X among the 17 elements were classified as X-rich (Hu et al., 2015; Zaizen et al., 2014). C-rich particles were identified based on the fact that the weight fraction of C as above 80% (Hu et al., 2016). Following this criterion, 214 particles in the samples collected in the haze period, 202 particles in the samples collected in the fog-haze period, and 216 particles in the samples of the clean period were characterized to explore the morphological and elemental changes, and their impact on HONO formation during haze evolution. The statistics of various particles in this study were based on their own number concentration (Bu et al., 2015).

3. Results and discussion

3.1. Meteorological interpretation and weather type identification

Fig. 1 illustrates the time series of meteorological parameters and the $PM_{2.5}$ concentration during the entire measurement period. Haze weather was identified by the criterion that visibility was lower than 10 km and RH was lower than 80%, whereas fog weather was termed when the visibility was lower than 10 km and RH was higher than 90% (Hu et al., 2015). When the visibility was higher than 10 km, the weather was defined as a clean day. As a result of the diurnal change of RH, the fog and haze episodes could transform each other within one day, and they were referred as a haze-fog episode (Shen et al., 2015). Based on this criterion, the meteorological conditions were firstly classified into four groups, as illustrated in Table 1. The first period (P1) was termed as the haze days, which occurred on 12th, 16th, 23rd and 24th of May, respectively. During this period, RH varied from 19 to 80%, and the $PM_{2.5}$ concentration ranged from 18 to 169 μg/m^3. The secondary period (P2) was identified as the haze-fog days, which occurred on 13rd, 14th, 15th, 22nd, 25th, and 28th of May, respectively. During this period, RH ranged between 62% and 96%, and $PM_{2.5}$ concentration ranged at 7–138 μg/m^3. According to the visibility data, the clean day was identified occurring on 17th, 19th and 20th of May, respectively, and were termed as the third period (P3). The $PM_{2.5}$ concentration showed relatively lower concentration and ranged from 7 to 82 μg/m^3 during this period. The rainfall period occurred on 21th, 26th and 27th of May, respectively, which was characterized by a rapid decrease of the $PM_{2.5}$ concentration via wet deposition, and was termed as the fourth period (P4).

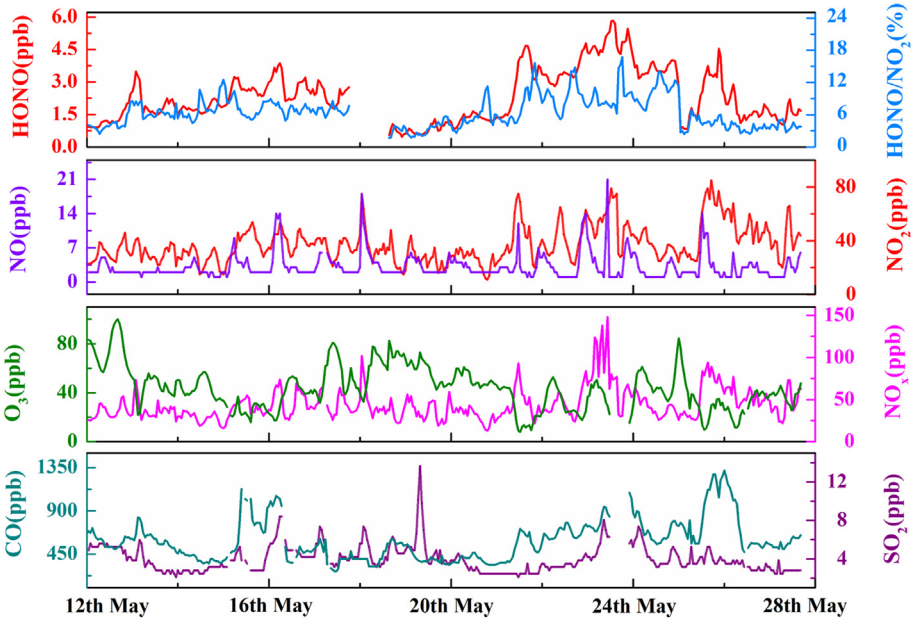

Fig. 2. Time series of HONO, NO, NO_2, O_3, CO, SO_2, and the HONO/NO_2 ratio.

Table 2
Comparisons of the HONO concentration in Shanghai and other sites around the world.

Observation sites	Period	HONO	Instruments	Reference
Houston, US (urban)	July-October, 2009	0.62	LOPAP	Rappenglück et al., 2013
Santiago, Chile (urban)	November 2009	1.44	IC	Rubio et al., 2009
Julich, Germany (urban)	June–July 2005	0.22	LOPAP	Elshorbany et al., 2012
Beijing, China (urban)	February–March 2002	1.49	LOPAP	Hou et al., 2016
Beijing, China (urban)	September 2015–July 2016	1.44	AIM-IC	Wang et al., 2017
Guangzhou, China (urban)	June 2006	2.80	DOAS	Qin et al., 2009
Xinken, China (suburban)	October–November 2004	1.30	WAD/IC	H·Su et al., 2008
Tung Chung, HK (suburban)	August–September 2011	0.35	LOPAP	Xu et al., 2015
Back Garden, China (rural)	July 2006	1.29	LOPAP	Li et al., 2012
Xi'an, China (urban)	July 2014-August 2015	1.04	LOPAP	Huang et al., 2017

3.2. Concentration and variation of the measured HONO

3.2.1. Temporal variations of HONO and relevant species

The HONO concentration profile and the relevant species during the entire measurement period are shown in Fig. 2. The HONO concentration ranged from 0.48 to 5.84 ppb and averaged at 2.31 ppb. The mean HONO concentration during P1, P2 and P3 were 2.80, 2.35 and 1.78 ppb, respectively. The maximum hourly value of HONO was 5.84 ppb, which was observed during P1 (at 0:00 on May 24). For comparison, the HONO level at other cities around the world is listed in Table 2. The averaged HONO level in the present study was higher than those reported in some foreign cities, such as Houston (0.62 ppb,

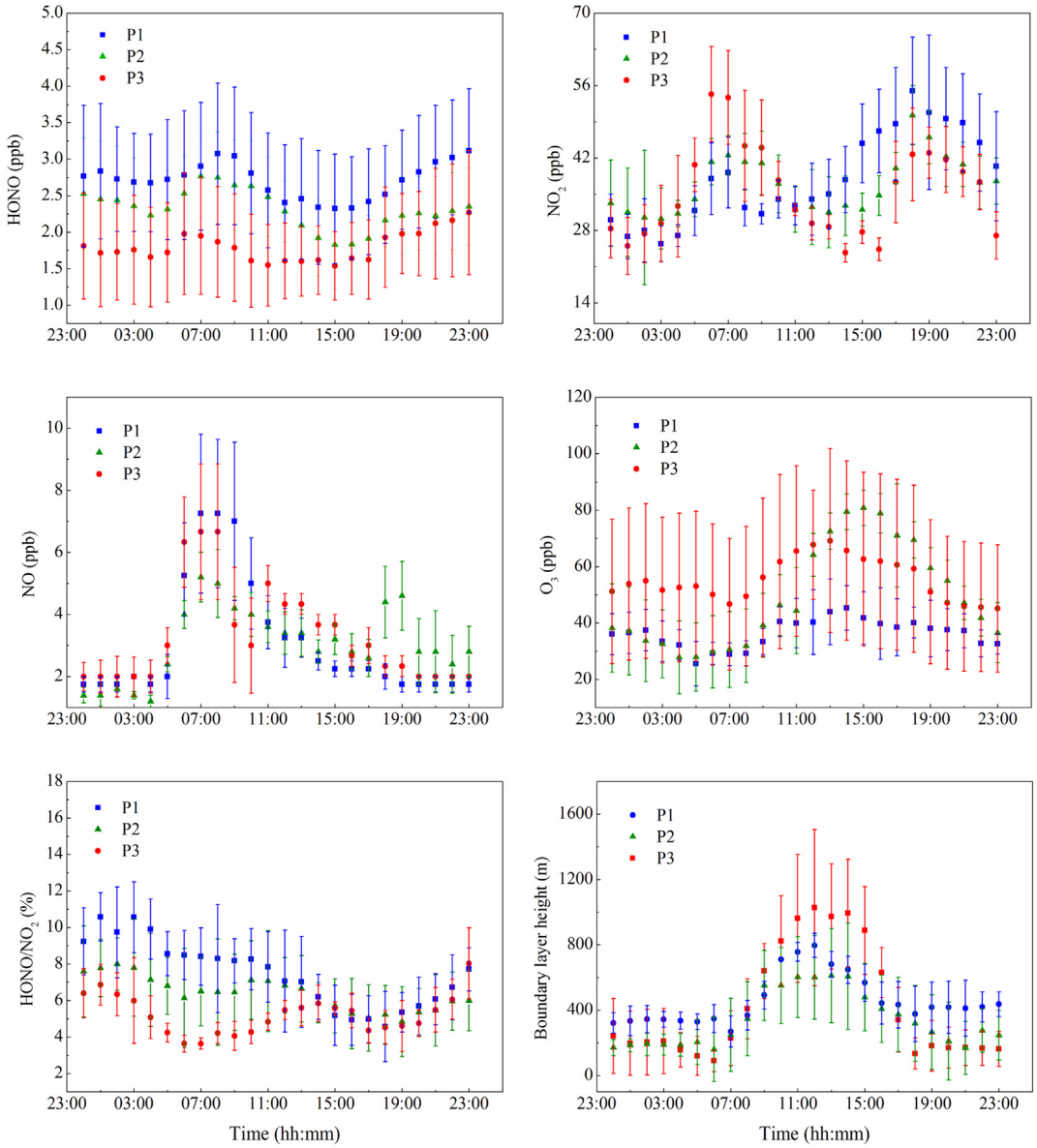

Fig. 3. Diurnal variations of HONO, NO_2, O_3, and the HONO/NO_2 ratio.

Rappenglück et al., 2013), Julich (0.22 ppb, Elshorbany et al., 2012), and Santiago (1.44 ppb, Rubio et al., 2009), and some urban areas in China including Beijing (1.49 ppb, Hou et al., 2016; 1.44 ppb, Wang et al., 2017) and Xi'an (1.04 ppb, Huang et al., 2017), but was lower than that measured in Guangzhou (2.80 ppb, Qin et al., 2009). The concentrations of NO_2 and O_3 ranged between 11 and 134 ppb and 7.93–99.87 ppb, respectively, during the entire measurement period, and averaged at 46.46, 32.67, 30.77 ppb, and 46.96, 40.13, 56.03 ppb, respectively, for P1, P2 and P3. The HONO/NO_2 ratio during the entire measurement period ranged from 0.13% to 17% and averaged at 6.17%. Considering the conversion from NO_2 to HONO, higher value of HONO/NO_2 could be expected for an aged air mass (Li et al., 2012). In the present study, the mean HONO/NO_2 ratios during P1, P2 and P3 were 8.03%, 7.48% and 5.18%, respectively.

The diurnal variations of HONO, NO_2,O_3, and the HONO/NO_2 ratio are illustrated in Fig. 3. To obtain valid diurnal variation patterns, the data during the rainfall period were excluded from the analysis. After sunset, HONO started to accumulate due to the attenuation of solar radiation and stabilization of the boundary layer (shown in Fig. 3), reaching the maximum values of 3.48, 3.16 and 1.97 ppb for P1, P2 and P3 in the morning, respectively. The HONO concentration decreased afterwards due to rapid photolysis and maintained at relatively low levels until sunset. The NO_2 concentration increased in the morning rush hours, then decreased rapidly and stayed at a low level in the afternoon in virtue of the development of the surface boundary layer. After sunset, NO_2 started to increase again, and the averaged nighttime NO_2 concentration remained at 43.4, 30.5 and 28.7 ppb for P1, P2 and P3, respectively. O_3 displayed a diurnal cycle opposite to HONO with maximum values of 45.3 54.8 and 72.0 ppb for P1, P2 and P3, respectively in the afternoon. The HONO/NO_2 ratio was commonly used to evaluate the HONO formation from the NO_2 conversion, which is less influenced by the diffusion during transport in the atmosphere as compared to the HONO value (Li et al., 2012). The HONO/NO_2 ratio started to increase after sunset and reached the peak during the nighttime, then it decreased in the early morning due to the enhancement of the NO_2 emission and the HONO photolysis. It should be noted that a small increase of HONO/NO_2 was observed at noontime for P3. Such phenomenon might be the result of the photo-enhanced redox reaction of NO_2 on particle surfaces (Shen and Zhang, 2013), and/or photolysis of particulate nitrate (NO_3^-) under the UV radiation (Zhou et al., 2002, 2003, 2011).

3.3. Nocturnal HONO sources

3.3.1. Direct emission

In the present study, the distances between the measurement site and the two main road, i.e. Handan Road and Wudong Road were about 150 m and 120 m, respectively, and the wind velocity ranged between 1 and 7 m/s. Accordingly, the respective air mass travel time over the two roads was estimated to be between 17 s and 2.5 min, which might be shorter than the daytime lifetime of HONO (15 s-30 min, Nie et al., 2015). Therefore, the measurement site might be affected by vehicular emissions. To estimate the upper limit of HONO emitted by traffic around the sampling site, the emission ratio (0.65%) of HONO/NO_2 obtained from the tunnel experiments by Kurtenbach et al. (2001) was widely applied in the recent studies (Qin et al., 2009; Tong et al., 2015). Therefore, the HONO concentration corrected by direct emission was calculated by the following equation:

$$[HONO]_{correct} = [HONO] - [HONO]_{emission} = [HONO] - 0.0065 \times [NO_x]. \quad (1)$$

Only the nighttime database was considered to avoid the influence of photolysis in the daytime. The frequency distribution of the $[HONO]_{emission}/[HONO]$ ratio during the measurement period is shown in Fig. S2. The calculated $[HONO]_{emission}/[HONO]$ ratio was 12.5% on average, implying that direct emissions were not an important HONO source in this study.

3.3.2. Homogeneous reaction of NO and OH

The homogeneous reaction of NO and OH was the dominant pathway for HONO formation in the gas phase, and the net HONO formation could be calculated by:

$$P_{net} = K_{NO+OH}[NO][OH] - K_{HONO+OH}[HONO][OH]. \quad (2)$$

The rate constant of K_{NO+OH} and $K_{HONO+OH}$ was 9.8×10^{-12} cm^3 $molecule^{-1}$ s^{-1} and 6.0×10^{-12} cm^3 $molecule^{-1}$ s^{-1} at 298 K, respectively (Atkinson et al., 2004; Sander et al., 2006). Since OH concentration was not measured in the present study, an average value of 1.0×10^6 molecules cm^{-3} measured in Beijing was assumed to represent the nighttime OH concentration of Shanghai (Tong et al., 2015), based on the similarity of simulated OH concentrations in these two cities (Lelieveld et al., 2016).

The diurnal variation cycle of the nocturnal P_{net} is illustrated in Fig. 4. Before midnight, the relatively low NO concentration (1.79 ppb) provided an average P_{net} value of 0.0080 ppb/h. After midnight, P_{net} showed an increase trend due to the increase of NO concentration and averaged at 0.020 ppb/h between 00:00 and 06:00. Since P_{net} is largely dependent on the OH concentration, the possible ranges of P_{net} was estimated by considering ±50% uncertainty of OH concentration. The averaged P_{net} was 0.0070 ppb/h (0.021 ppb/h) for −50% (+50%) changes of OH concentration, which is within the range of the values observed in other areas of China (Li et al., 2012; Spataro et al., 2013).

3.3.3. Heterogeneous conversion of NO_2 to HONO

Field measurements in many urban sites found positive correlation between HONO and NO_2, indicating that NO_2 may be an important HONO precursor (Spataro et al., 2013; Wang et al., 2013; Huang et al., 2017; Qin et al., 2009). The averaged HONO/NO_2 ratio of 6.2% measured in this work is much larger than the reported value of 1% from direct emissions (Kurtenbach et al., 2001), suggesting that heterogeneous reaction could be a more important pathway for HONO production compared to direct emissions. In the present study, HONO exhibited a moderate but significant correlation with NO_2 ($R^2 = 0.58$, $p < 0.01$),

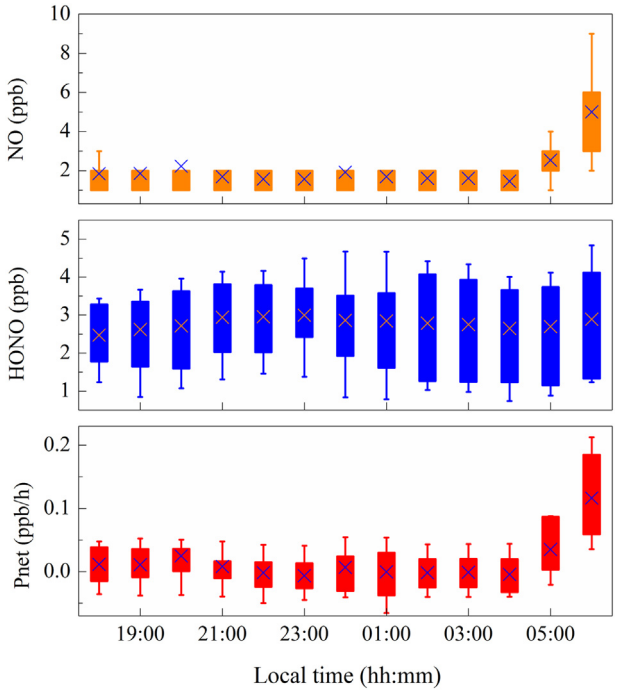

Fig. 4. Mean nocturnal variation of P_{net}, NO and HONO. These box-whisker diagram were based on 1 h averages for the time intervals where both measurements were present. The "×" symbol refers to the average value, boxes and whiskers represents the 25%–75% and 90% of the data.

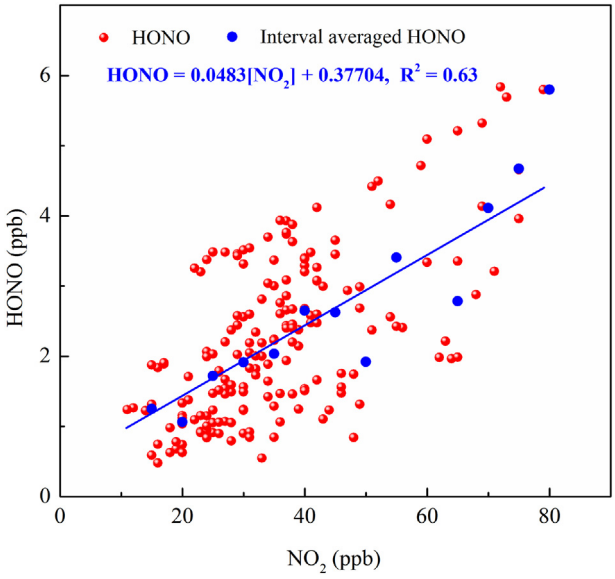

Fig. 5. The relationship between HONO and NO_2 at night.

indicating the importance of heterogeneous conversion from NO_2 to HONO (Fig. 5).

For the heterogeneous conversion of NO_2, the surface of soot particle as a media has been reported by several studies (Shen and Zhang, 2013; An et al., 2014). It was well known that the contribution of soot surface to HONO production is often much less than that expected, due to the fact that the uptake efficiency of NO_2 decreased with prolonged reaction time due to the surface deactivation. Aerosol surface was assumed to be an important media for the heterogeneous conversion of NO_2 to HONO (Liu et al., 2014; Li et al., 2012). Herein, aerosol mass concentration was used as a surrogate to identify the aerosol influence on HONO formation (Park et al., 2004; Hao et al., 2006). Fig. 6a shows the correlation between the mass concentration of $PM_{2.5}$ and the HONO/NO_2 ratio. One can see that the mean HONO/NO_2 ratio increased gradually with increasing $PM_{2.5}$ level, indicating that aerosol surfaces played a vital role on the heterogeneous conversion of NO_2 to HONO.

Stutz et al. (2004) pointed out that the absorbed water exerted the influence on heterogeneous formation of HONO. The effect of RH on the heterogeneous conversion of NO_2 to HONO is illustrated in Fig. 6b. The HONO/NO_2 ratio increased with the increasing RH from 40% to 75%, whereas further increase of RH led to the decrease of the HONO/NO_2 ratio. Similar variation patterns were frequently observed in the previous studies (Yu et al., 2009; Qin et al., 2009; Wang et al., 2013; Huang et al., 2017). The absorbed water on surfaces could serve as both the source and sink of HONO by affecting the HONO production from NO_2 hydrolysis and HONO deposition (Ammann et al., 1998). When RH was in the range of 40% to 75%, the moisture effect on the heterogeneous conversion of NO_2 to HONO was stronger than the HONO deposition, thus the conversion efficiency increased (Stutz et al., 2004). However, once the surface reached saturation state (RH > 75%), the excess water on the surface could become a limiting reagent for the NO_2 conversion (Wojtal et al., 2011). Instead, the uptake and dissolution of HONO by water layer on saturated surfaces could lead to the decrease in the HONO/NO_2 ratio.

The conversion frequency (C_{HONO}) of HONO was generally used as an indicator to evaluate the conversion rate of NO_2. It was supposed that all of HONO was produced by the heterogeneous conversion of NO_2 (Hou et al., 2016), and the C_{HONO} value could be calculated by Eq. (2) (Alicke et al., 2003; Su et al., 2008).

$$C_{HONO} = ([HONO]_{t2} - [HONO]_{t1})/(t2 - t1)[NO_2]. \quad (3)$$

where [NO_2] means the average NO_2 concentration during the time interval from t1 to t2.

The heterogeneous conversion rate of NO_2 was 1.14×10^{-2} h^{-1} on average. C_{HONO} was compared with that reported in the other places around the world (Fig. S3). The conversion rate in the present study was lower than that reported at urban Guangzhou (Li et al., 2012), but was higher than that observed at urban Jinan (Wang et al., 2015), urban Xi'an (Huang et al., 2017), and rural Hongkong (Xu et al., 2015). The averaged C_{HONO} value was 1.58×10^{-2} h^{-1} in the pollution period, which was much higher than that in the clean period (0.93×10^{-2} h^{-1}). The enhanced conversion rate indicated higher reaction efficiency of NO_2 via the heterogeneous process during the haze and fog, which may be associated with the higher aerosol surface due to high particle loading, and/or higher water content on the particle surface due to higher RH (Xu et al., 2015).

3.4. Daytime HONO budget

Based on the production and loss processes of HONO, the daytime HONO formation rate can be expressed by:

$$\frac{dHONO}{dt} = (P_{emi} + P_{NO+OH} + P_{het} + P_{unknown}) - (L_{HONO+OH} + L_{pho} + L_{dep}) + T_v. \quad (4)$$

where dHONO/dt represents the variation of HONO concentration within the time interval of Δt. P_{emi}, $P_{NO+OH,}$ P_{het} and $P_{unknown}$ donate

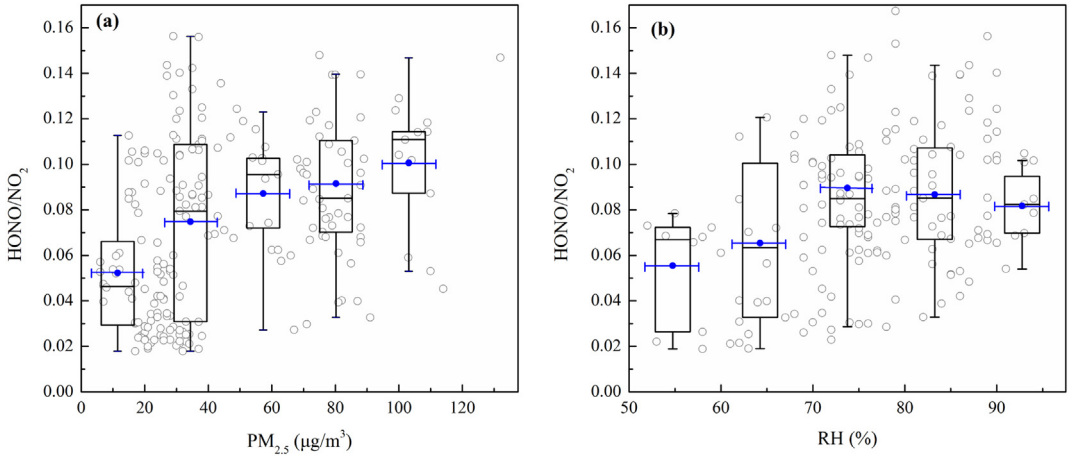

Fig. 6. The correlations between $HONO_{correct}/NO_2$ and RH (a) and $PM_{2.5}$ concentration (b) at night.

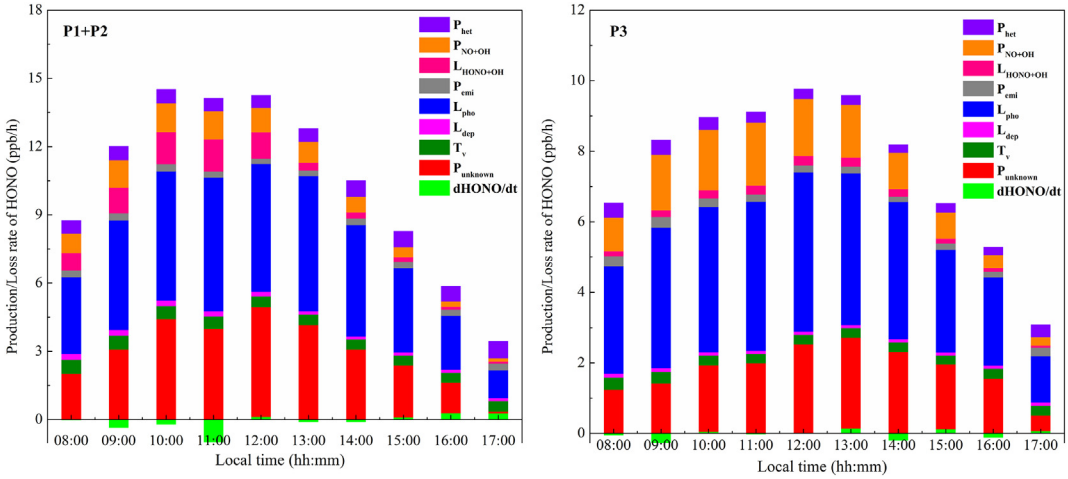

Fig. 7. Averaged production and loss rates for the daytime HONO budget during the pollution period and the clean period.

the formation rate of direct emissions, the gas-phase reaction of NO and OH, the dark heterogeneous conversion of NO_2, and the additional unknown daytime HONO, respectively. $L_{HONO+OH}$, L_{pho}, L_{dep} and Tv are the loss rate of HONO through reaction with OH, the photolysis of HONO, the dry deposition of HONO, and vertical advection, respectively. L_{pho} could be expressed as: $L_{pho} = J_{HONO} \times [HONO]$, where J_{HONO} is the photolysis frequency of HONO. L_{dep} was estimated by $V_d \times [HONO] / H$, where V_d is the dry deposition velocity of HONO and H is the mixing height. Vd was 2.0 cm/s, given by Harrison et al. (1996). The magnitude of Tv could be estimated by using a parameterization for dilution by background air provided by Dillon et al. (2002):

$$Tv = k_{(dilution)} \left([HONO] - [HONO]_{background} \right). \quad (5)$$

The $k_{(dilution)}$ was 0.23 h^{-1} as given by Dillon et al. (2002), and the [HONO] background value was about 10 ppt according to Zhang et al. (2009). Therefore, the daytime unknown HONO production rate was calculated by:

$$P_{unknown} = \frac{dHONO}{dt} + L_{pho} + L_{dep} + L_{HONO+OH} - P_{NO+OH} - P_{emi} - P_{het} - T_v. \quad (6)$$

Since measurements of photolysis frequencies and OH concentration were not available in this study, the TUV model (http://www.acd.ucar.edu/TUV) was adopted to calculate the photolysis frequencies and OH concentration. The ozone density, aerosol optical depth (AOD), single scattering albedo (SSA) and Ångström exponent (Alpha) are important input parameters influencing the J value in the TUV model. The ozone density was measured by Total Ozone Mapping Spectrometer (http://toms.gsfc.nasa.gov/teacher/ozoneoverhead.html). The typical AOD, SSA and Alpha values during clean and pollution period were 0.66, 0.89, 1.07, and 1.32, 0.90, 1.30, respectively (Cheng et al., 2015; Xu et al., 2012; Lv et al., 2017; Lei et al., 2013; Tang et al., 2014). The daytime OH concentration was calculated by applying the method proposed by Rohrer and Berresheim (2006). The calculated OH concentrations during the pollution period and the clean period was 5.74×10^6 molecules cm^{-3} and 7.06×10^6 molecules cm^{-3}, respectively. These values were in the range of $(0.5–2) \times 10^7$ cm^{-3} in Chinese urban environment during summertime, but were higher than the values observed during wintertime (Kanaya et al., 2007; Lu et al., 2012; Lu et al., 2013).

The calculated HONO production rate relating to gas phase production, direct emission, and the unknown source are illustrated in Fig.7. The averaged daytime P_{emi}, P_{NO+OH}, P_{het} and $P_{unknown}$ in the pollution period and the clean period were 0.28, 0.83, 0.62, 2.98 and 0.21, 1.15, 0.30, 1.78 ppb/h, respectively, indicating that $P_{unknown}$ was the dominant HONO source in the daytime. The existence of unknown HONO sources invoked the question about the underlying HONO formation mechanisms in the atmosphere. To characterize the role of aerosol surface in daytime unknown HONO sources, the relationship between

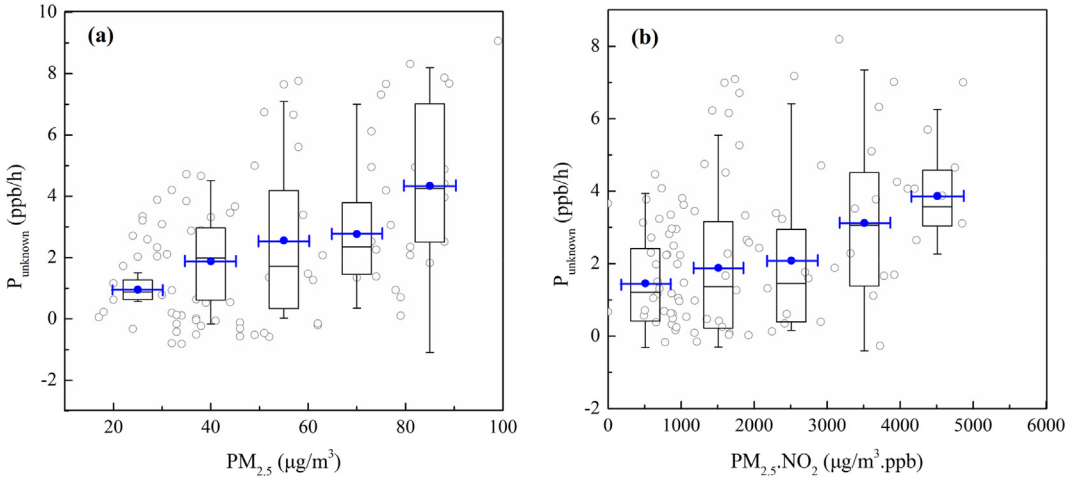

Fig. 8. The correlations between $P_{unknown}$ and $PM_{2.5}$ (a) and $PM_{2.5} \times NO_2$ (b).

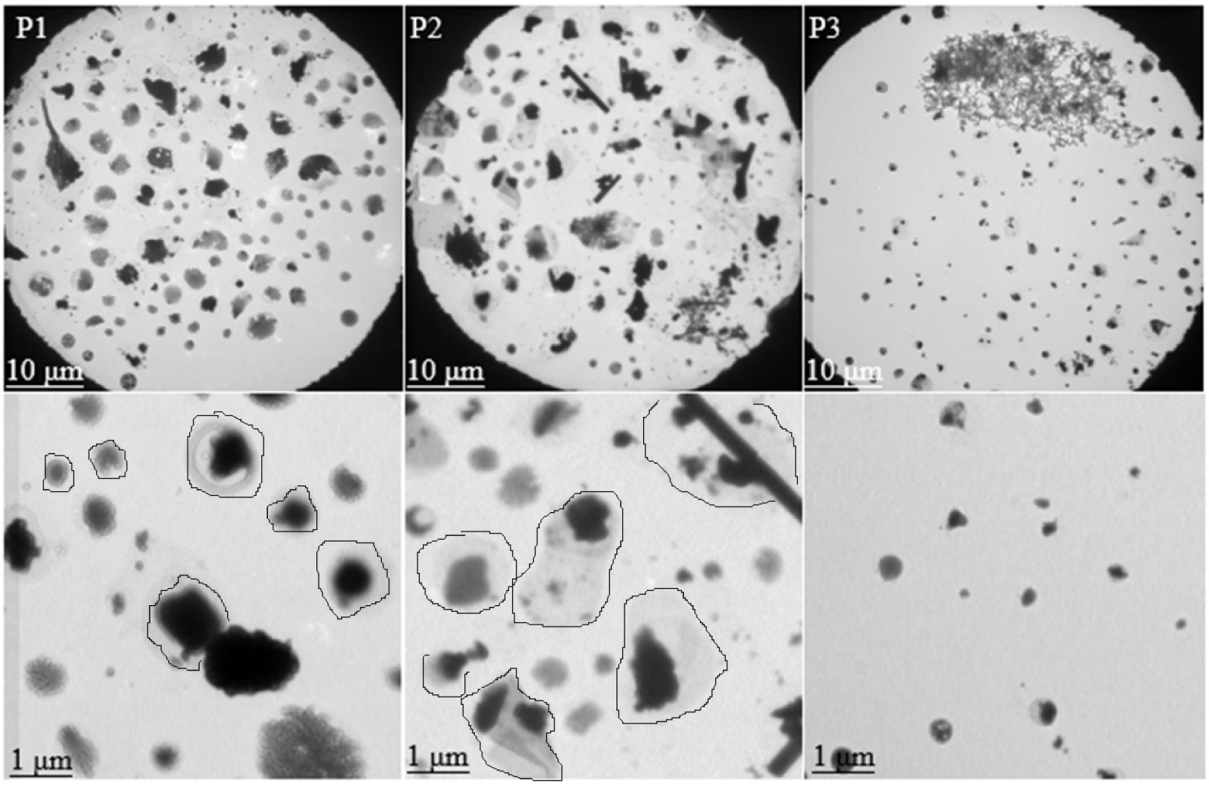

Fig. 9. TEM images of aerosol particles from the haze, fog and clear days.

$P_{unknown}$ and $PM_{2.5}$ was analyzed. As illustrated in Fig. 8, the $P_{unknown}$ valueincreased gradually with the increase of $PM_{2.5}$ concentration and the value of $PM_{2.5} \times [NO_2]$, suggesting that the heterogeneous conversion of NO_2 on aerosol surfaces could contributed as a missing daytime HONO source during the transformation of the clean period to the haze/fog period.

3.5. Single particle analysis

3.5.1. Morphological identifications of aerosols during the different weather types

The particle specific surface area associated with the particle size distribution and morphology is an important parameter influencing the transformation of NO_2 to HONO (Nie et al., 2015). As shown in Fig. 9, the particles displayed diversified morphologies for different weather types. Most of the particles collected during P1 and P2 were agglomerated, whereas the particles during P3 were uniformly distributed. WS was relatively higher during P3 as compared to that during P1 and P2 (shown in Table 1). The relatively better diffusion condition in the clean period decreased the retention time of aerosols in the atmosphere, resulting in the less chance of the collision and combination among the aerosol particles (Hu et al., 2016). This result suggested that haze aerosols have a larger particle size than clean samples, which is caused by a higher number of agglomerated state particles, and favor NO_2 to HONO at a similar level of the particle mass concentration.

Under the TEM, the water-film mark was clearly seen on the edges of most samples during P1 and P2, suggesting that RH in the atmosphere exceeded the deliquescence relative humidity (DRH) of these particles, and liquid layer could be formed around the deliquesced particles. Such property was mainly observed at the cycling of haze-fog transformation for the ageing process (Hu et al., 2016). It was well documented that the liquid layer formed on particle surfaces could affect the gas-aerosol equilibrium by changing the equilibrium balance to benefit the uptake of NO_2 (You et al., 2012). As shown in Table 1, higher RH was coupled

Table 3
Classification of the different particle types, morphologies, mixing states and sources of the individual particles.

Particle types	Possible particle phases	Morphology	Mixing properties	Sources
Mineral dust	Quartz and calcite	Elongate regular shapes with sizes smaller than 1 μm	Reacted minerals contained secondary formed $CaSO_4$ and $Ca(NO_3)_2$	Road dust and/or other anthropogenic sources including construction dust and cement industry
K-rich	Irregular K_2SO_4 and KNO_3	Irregular morphology	Externally mixed with metals	Biomass burning
Na-rich	Viscous $Na_2SO_4/NaNO_3$	Amorphous structure with	Mixed with fly ash	Aged particles of NaCl
Metal/Fly ash	Metal: Fe-rich, Zn-rich and Al-rich particles; fly ash: spherical Fe-rich containing Zn, Na, and Si.	Nearly spherical shapes with sizes mostly smaller than 100 nm	Inclusions of secondary sulfates and nitrates	Industries, coal-fired power plant, and waste incineration.
N/S bearing	$(NH_4)_2SO_4$ and NH_4NO_3	Scallop-like or "bubbly" microstructures	Mixed metal/fly ash, mineral particles	Secondary particles formed by SO_2 and NO_x
Soot	Graphitic spherules	Chain-like aggregates of carbon-bearing spheres	Mixed with N/S bearing particles	Fossil fuels and/or biomass burning

with higher concentrations of NO_2 during P1 and P2. Such condition could promote the heterogeneous reaction of NO_2 on wet surfaces of particles to yield HONO, HNO_3, and nitrates (Krueger et al., 2003, 2004; Geng et al., 2014; Li and Shao, 2009):

$$2NO_2(g) + H_2O(abs) \rightarrow HONO(g) + HNO_3(g). \quad (7)$$

3.5.2. Classification of aerosols during P1, P2 and P3

Besides the particle size and morphology, the chemical nature of aerosols, which could control the NO_2 conversion efficiency, is also a candidate influencing the transformation of NO_2 to HONO. Based on elemental composition and morphology of individual particle, seven different particle types were identified: mineral, metals, fly ash, soot, K-rich, Na-rich and S/N bearing particles. The particle characteristics, mixing states and sources of different particle types were illustrated in Table 3. Mineral particles showed irregular shapes, and they were categorized into silicon-rich and calcium-rich particles based on the EDS data (Fig. 10a–d). Metals were sorted out into two major clusters: Zn-rich (Fig. 10f) and Fe-rich (Fig. 10g–j) particles. Fly ash (Fig. 10k) particles contained Al and Si with minor Fe. Most metal/fly ash particles exhibited spherical morphology under the TEM, suggesting that they were derived from high-temperature processes (Li et al., 2016). Soot particles displayed onion-like structure of graphitic layers (Fig. 10l). K-rich

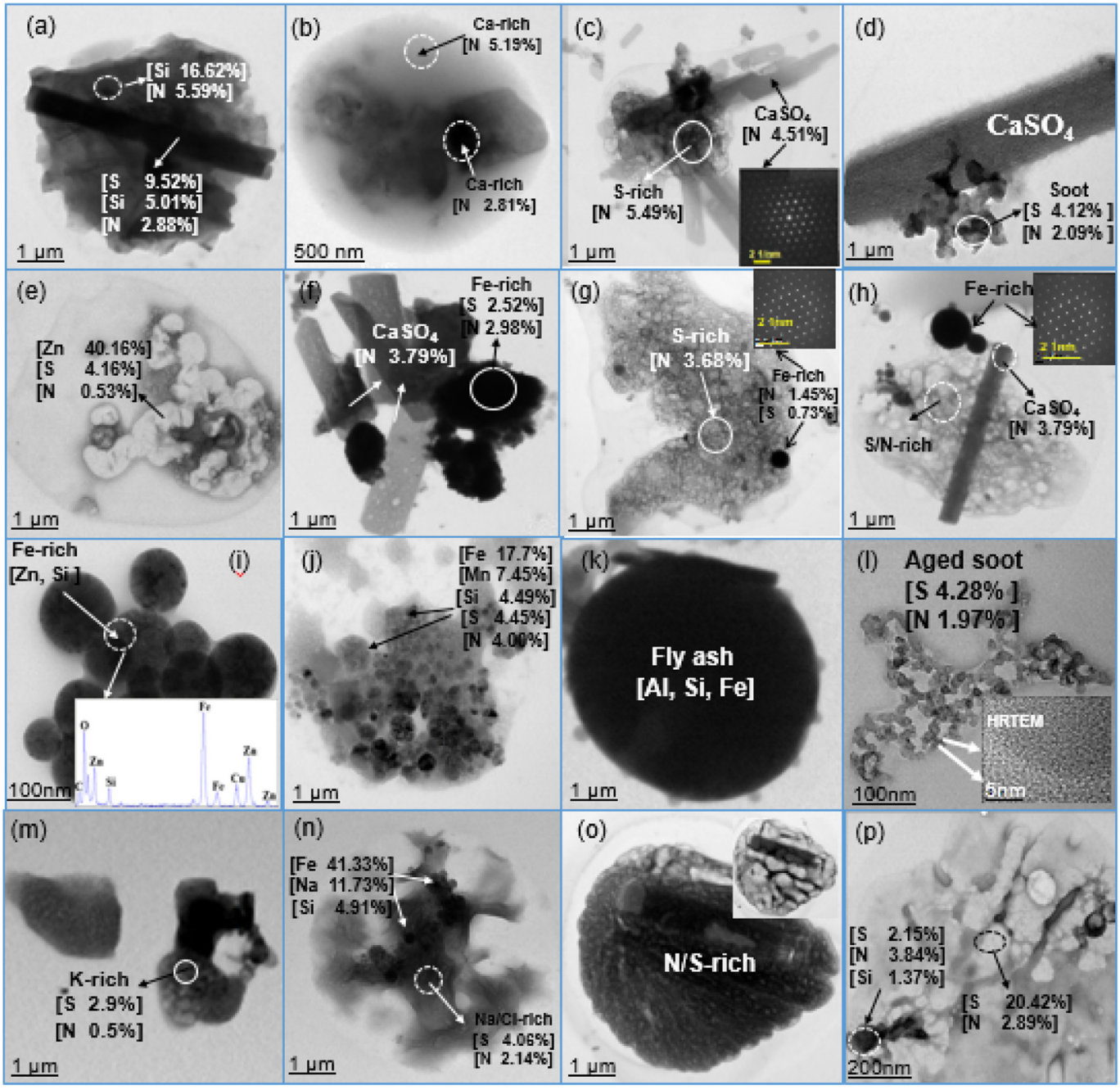

Fig. 10. Various types of the individual particles in the Shanghai atmosphere identified by TEM/EDS. (a) Spherical Si-rich particle coated with S and N. (b) and (c) Ca-rich particle with S/N coatings. (d) Aggregated Ca-rich particles and soot. (e) Spherical Al- rich particle. (f) Zn-rich particles mixing with S and N. (g) and (h) Aggregated Fe-rich and Ca-rich particles, which were internally mixed with minor N and S. (i) Spherical Fe-rich particles with S/N coating. (j) Fe-Zn rich particle (k) Fly ash, which constituted mainly Fe, Mn, Si, S and N. (l) Aggregates of chain-like soot particles with minor N and S. (m) Irregular K-rich particles, which were internally mixed with the S and N elements. (n) Internally mixed fly ash and the Na-rich particle. (o) and (p) the S/N-bearing particle, which were sensitive and volatilized under the TEM.

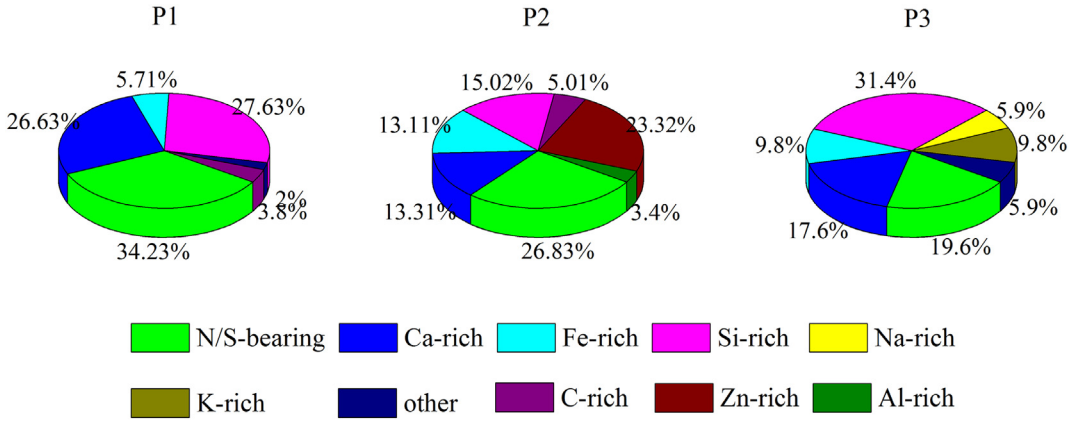

Fig. 11. Relative number abundances of various particle types during the measurement period.

particles exhibited irregular shapes (Fig. 10m). Fig. 10n showed aggregates of metals and Na-rich particles, which indicated that aerosol particles were collided and amalgamated with each other during the retention in the atmosphere. S/N-bearing particles displayed "bubbly" appearances (Fig. 10o and p), due to that they were sensitive to the strong electric beams and vaporized within a few seconds. It should be noted that N and S were detected internally mixed with minerals, metals/fly ash, soot and K-rich particles, indicating heterogeneous reactions of NO_2 and SO_2 on these particle surfaces.

Fig. 11 showed that the S/N bearing particles dominated over other particle types during P1 and P2, and number percentages accounted for 34% and 27%, respectively. For the samples collected during P3, the S/N bearing particles showed a lower proportion (20%) in number. Such particles were commonly identified as $(NH_4)_2SO_4/NH_4HSO_4$, and NH_4NO_3, which are transformed from trace gases of NO_2, SO_2 and NH_3 in the atmosphere (Li et al., 2013). In the nucleation procedure of NO_2, H_2O and NH_3, HONO is generated as a main product (Li and Shao, 2009; Zhang and Tao, 2010):

$$2NO_2(g) + H_2O(g) + NH_3(g) \rightarrow HONO(g) + NH_4NO_3(s). \quad (8)$$

The higher proportion of such particles during the pollution episodes suggested higher HONO formation potential from this reaction.

As mentioned above, substantial minerals (e.g., Ca and Si) and metals (Fe and Zn) were internally mixed with nitrogen, indicating that such particles were involved in heterogeneous processes with NO_2 and converted into hydrophilic nitrates during the long-range transport in the atmosphere (Alexander et al., 2009; Li and Shao, 2009; Sullivan et al., 2007). The relative abundance of internally mixed particles was 84%, 79% and 52%, respectively, for aerosol samples during P1, P2 and P3. Fresh mineral and metallic particles in the atmosphere are hydrophobic, however, these particles could become hydrophilic when they wre mixed with hydrophilic species and enhance the uptake capacity of water and some gases on these particles (Krueger et al., 2003, 2004; Fountoukis and Nenes, 2007). From this view point it was expected that the nitrates formed in these particles could further benefit for enhanced HONO production on particle surfaces. Aerosols with different chemical compositions could be used to evaluate atmospheric processes. In our samples, the average ratios of N/Ca, N/Si and N/Fe collected during P1 and P2 was 0.21, 1.03, 0.31, and 0.26, 0.53, 0.24, respectively, whereas those during the clean period were 0.11, 0.30, and 0.09, respectively (Fig. 12). These results indicated that the hydrolysis of NO_2 to HONO and NO_3^- could be promoted during the haze/fog episodes at the relatively high RH.

In conclusion, the surface areas and chemical nature of particles are the dominant factors to influence the conversion potential of NO_2 to HONO. The enhanced particle loadings along with enlarged particle sizes, characterizing by higher number of agglomerated state particles were observed in the pollution episodes. In consequence, the NO_2 uptake efficiency and the HONO production capacity could be enhanced at the similar levels of the PM mass concentration (Janhäll et al., 2010). In this work, the high abundance of minerals and transition metals, which are high-performance media for converting NO_2 to HONO, should promote the HONO production during the age in the atmosphere. Besides, since most minerals and metals were mixed with sulfates and nitrates synchronously (Fig. 10), the heterogeneous conversion of NO_2 on these aerosol surfaces could be accelerated due to that the highly hygroscopic sulfates could facilitate the uptake of water and the NO_2 hydrolysis on particles surfaces (Twohy and Anderson, 2008; Zhang et al., 2006; Stutz et al., 2004). In the present study, the averaged $HONO/NO_x$ ratios were 5.6%, especially during the haze (8.0%) and haze-fog (7.3%) episodes were much higher than the

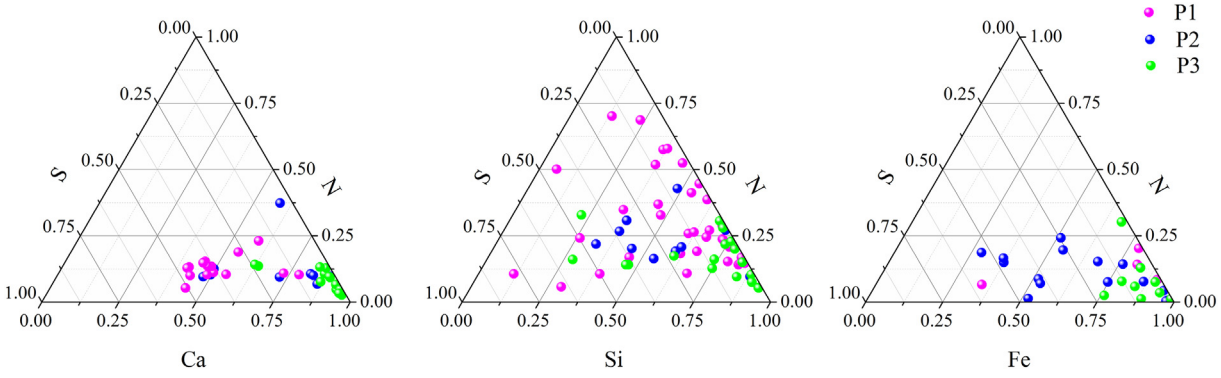

Fig. 12. Ternary diagram of C-N-S of mineral (Ca, Si) and metallic (Fe) aerosols particles during P1, P2 and P3.

assumed global averaged value of 2.0% (Elshorbany et al., 2012; Elshorbany et al., 2014), implicating a potentially important role for the HONO chemistry at Shanghai.

4. Conclusions

Ambient HONO measurement was carried out in the downtown of Shanghai, China using an in-situ LOPAP instrument. The HONO concentrations during P1, P2 and P3 were 2.80, 2.35 and 1.78 ppb, respectively. Heterogeneous conversion of NO_2 was the dominant nocturnal HONO formation pathway. The HONO/NO_2 ratio during P1, P2 and P3 were 8.03%, 7.48% and 5.18%, respectively. The averaged C_{HONO} value during the pollution episodes (1.58×10^{-2} h^{-1}) was higher than that during the clean period (0.91×10^{-2} h^{-1}). This implied higher heterogeneous conversion potential of NO_2 to HONO during the pollution episodes. The HONO/NO_2 ratio increased with the $PM_{2.5}$ concentration increasing, indicating that aerosol played an important role for heterogeneous conversion of NO_2 to HONO. Daytime HONO budget analysis showed that the average $P_{unknown}$ during the pollution period and the clean period was 2.98 ppb/h and 1.78 ppb/h, respectively. Further, $P_{unknown}$ was found to be closely associated with the $PM_{2.5}$ concentration. Under the TEM, enlarged particle sizes for the haze and fog samples were observed, which could be elucidated by a higher number of the agglomerated state particles. The number percentage of the *S*/*N*-bearing particles during P1 (34%) and P2 (27%) were higher than that during P3 (20%). In addition, 84%, 79%, and 52% by number of minerals and transition metals were detected internally mixed with nitrogen, suggesting the elevation of HONO production from airborne sources during the haze episodes, which could be contributed by higher particle loadings and larger particle surfaces. In this study, the averaged HONO/NO_x ratios was 5.60%, especially during the haze (7.80%) and haze-fog (7.50%) episodes were considerably higher than that assumed global averaged value of 2.0%, suggesting a potential important role for HONO chemistry in Shanghai, especially during haze episodes.

Acknowledgments

This work was supported by the National Key R&D Program of China (2016YFC0202700), National Natural Science Foundation of China (Nos. 91744205, 21777025, 21577022, 21177026), Marie Skłodowska-Curie Actions (690958-MARSU-RISE-2015) and International cooperation project of Shanghai Municipal Government (15520711200).

Appendix A. Supplementary data

Supplementary data to this article can be found online at https://doi.org/10.1016/j.scitotenv.2018.02.063.

References

Acker, Karin., Möller, Detlev., Wieprecht, Wolfgang., Meixner, Franz X., Bohn, Birger., Gilge, Stefan., Plass-Dülmer, Christian., Berresheim, Harald, 2006. Strong daytime production of OH from HNO_2 at a rural mountain site. Geophys. Res. Lett. 33, L02809. https://doi.org/10.1029/2005GL024643.

Alexander, B., Park, R.J., Jacob, D.J., Gong, S., 2009. Transition metal-catalyzed oxidation of atmospheric sulfur: global implications for the sulfur budget. J. Geophys. Res. 114.

Alicke, B., Geyer, A., Hofzumahaus, A., 2003. OH formation by HONO photolysis during the BERLIOZ experiment. J. Geophys. Res. 108, 17.

Ammann, M., Kalberer, M., Jost, D.T., 1998. Heterogeneous production of nitrous acid on soot in polluted air masses. Nature 395, 157–160.

Ammann, M., Rossler, E., Strekowski, R., George, C., 2005. Nitrogen dioxide multiphase chemistry: uptake kinetics on aqueous solutions containing phenolic compounds. Phys. Chem. Chem. Phys. 7, 2513–2518.

An, J., Zhang, W., Qu, Y., 2009. Impacts of a strong cold front on concentrations of HONO, HCHO, O^3, and NO_2 in the heavy traffic urban area of Beijing. Atmos. Environ. 43 (22-23), 3454–3459.

An, J., Li, Y., Wang, F., Xie, P., 2011. Impacts of photoexcited NO_2 chemistry and heterogeneous reactions on concentrations of O_3 and NO_y in Beijing, Tianjin and Hebei Province of China. In: Mazzeo, Nicolas (Ed.), Air Quality-Models and Applications (ISBN 978-953-307-307-1).

An, J., Li, Y., Chen, Y., Li, J., Qu, Y., Tang, Y., 2013. Enhancements of major aerosol components due to additional HONO sources in the North China Plain and implications for visibility and haze. Adv. Atmos. Sci. 30 (1), 57–66.

An, J.L., Li, Y., Tang, Y.J., Chen, Y., 2014. Advances in HONO sources, HONO simulations, and the impact of the HONO sources on regional or global air. China Environ. Sci. 34 (2), 73–281.

Atkinson, R., Baulch, D.L., Cox, R.A., Crowley, J.N., Hampson, R.F., Hynes, R.G., Jenkin, M.E., Rossi, M.J., Troe, J., 2004. Evaluated kinetic and photochemical data for atmospheric chemistry: volume I-gas phase reactions of Ox, HOx, NOx and Sox species. Atmos. Chem. Phys. 4:1461–1738. https://doi.org/10.5194/acp-4-1461-2004.

Aubin, D.G., Abbatt, J.P.D., 2007. Interaction of NO_2 with hydrocarbon soot: focus on HONO yield, surface modification, and mechanism. J. Phys. Chem. A 111, 6263–6273.

Bu, D., Zhang, Y.C., Kong, L.D., Fu, H.B., Hu, Y.J., Chen, J.M., Li, L., Qiong, A., 2015. Individual particle analysis of aerosols collected at Lhasa City in the Tibetan Plateau. J. Environ. Sci. 29, 165–177.

Chan, C.K., Yao, X., 2008. Air pollution in mega cities in China. Atmos. Environ. 42, 1–42.

Cheng, T.T., Xu, C., Duan, J.Y., Wang, Y.F., Leng, C.P., Tao, J., Che, H.Z., He, Q.S., Wu, Y.F., Zhang, R.J., Li, X., Chen, J.M., Kong, L.D., Yu, X.N., 2015. Seasonal variation and difference of aerosol optical properties in columnar and surface atmospheres over Shanghai. Atmos. Environ. 123, 315–326.

Czader, B.H., Rappenglück, B., Percell, P., Byun, D.W., Ngan, F., Kim, S., 2012. Modeling nitrous acid and its impact on ozone and hydroxyl radical during the Texas Air Quality Study 2006. Atmos. Chem. Phys. 12 (15):6939–6951. https://doi.org/10.5194/acp-12-6939-2012.

Dillon, M.B., Lamanna, M.S., Schade, G.W., Goldstein, A., Cohen, R.C., 2002. Chemical evolution of the Sacramento urban plume: transport and oxidation. J. Geophys. Res. 107, 4045. https://doi.org/10.1029/2001JD000969.

Duplissy, J., Gysel, M., Alfarra, M.R., Dommen, J., Metzger, A., Prevot, A.S.H., Weingartner, E., Laaksonen, A., Raatikainen, T., Good, N., Turner, S.F., McFiggans, G., Baltensperger, U., 2008. Cloud forming potential of secondary organic aerosol under near atmospheric conditions. Geophys. Res. Lett. 35, L03818. https://doi.org/10.1029/2007GL031075.

Elshorbany, Y.F., Steil, B., Bruehl, C., 2012. Impact of HONO on global atmospheric chemistry calculated with an empirical parameterization in the EMAC model. Atmos. Chem. Phys. 12 (20), 9977–10000.

Elshorbany, Y.F., Crutzen, P.J., Steil, B., Pozzer, A., Tost, H., Lelieveld, J., 2014. Global and regional impacts of HONO on the chemical composition of clouds and aerosols. Atmos. Chem. Phys. 14:1167–1184. https://doi.org/10.5194/acp-14-1167-2014.

Feng, Y., Chen, Y., Guo, H., Zhi, G., Xiong, S., Li, J., 2009. Characteristics of organic and elemental carbon in $PM_{2.5}$, samples in Shanghai, China. Atmos. Res. 92 (4), 434–442.

Finlayson-Pitts, B.J., Wingen, L.M., Sumner, A.L., Syomin, D., Ramazan, K.A., 2003. The heterogeneous hydrolysis of NO_2 in laboratory systems and in outdoor and indoor atmospheres: an integrated mechanism. Phys. Chem. Chem. Phys. 5 (2), 223–242.

Fountoukis, C., Nenes, A., 2007. ISORROPIA II: a computationally efficient thermodynamic equilibrium model for K^+-Ca^{2+}-Mg^{2+}-NH_4^+-Na^+-SO_4^{2-}-NO_3^--Cl^--H_2O aerosols. Atmos. Chem. Phys. 7, 4639–4659.

Fu, H., Zhang, M., Li, W., Chen, J., Wang, L., Quan, X., Wang, W., 2012. Morphology, composition and mixing state of individual carbonaceous aerosol in urban Shanghai. Atmos. Chem. Phys. 12, 693–707.

Fu, H.B., Chen, J.M., 2017. Formation, features and controlling strategies of severe haze-fog pollutions in China. Sci. Total Environ. 578, 121–138.

Genfa, Z., Slanina, S., Boring, C.B., Jongejan, P.A.C., Dasgupta, K., 2003. Continous wet denuder measurements of atmospheric nitric and nitrous acid during the 1999 Atlanta supersite. Atmos. Environ. 37, 1351–1364.

Geng, H., Hwang, H., Liu, X., Dong, S., Ro, C.U., 2014. Investigation of aged aerosols in size-resolved Asian dust storm particles transported from Beijing, China, to Incheon, Korea, using low-Z particle EPMA. Atmos. Chem. Phys. 14, 3307–3323.

Grassian, 2002. Chemical reactions of nitrogen oxides on the surface of oxide, carbonate, soot, and mineral dust particles: implications for the chemical balance of the troposphere. J. Phys. Chem. A 106, 860–877.

Guo, S., Hu, M., Zamora, M.L., Peng, J., 2014. Elucidating severe urban haze formation in China. Proc. Natl. Acad. Sci. U. S. A. 111 (49), 17373–17378.

Han, C., Yang, W.J., Wu, Q.Q., Yang, H., Xue, X.X., 2016. Heterogeneous photochemical conversion of NO_2 to HONO on the humic acid surface under simulated sunlight. Environ. Sci. Technol. 50, 5017–5023.

Han, D.M., Wang, Z., Cheng, J.P., Wang, Q., Chen, X.J., Wang, H.L., 2017. Volatile organic compounds (VOCs) during non-haze and haze days in Shanghai: characterization and secondary organic aerosol (SOA) formation. Environ. Sci. Pollut. Res. 24, 18619–18629.

Hao, N., Zhou, B., Chen, D., Chen, L.M., 2006. Observations of nitrous acid and its relative humidity dependence in Shanghai. J. Environ. Sci. 18 (5), 910–915.

Harrison, R.M., Peak, J.D., Collin, G.M., 1996. Tropospheric cycle of nitrous acid. J. Geophys. Res. 101, 14429–14439.

Heland, J., Kleffmann, J., Kurtenbach, R., Wiesen, P., 2001. A new instrument to measure gaseous nitrous acid (HONO) in the atmosphere. Environ. Sci. Technol. 35, 3207–3212.

Hendrick, F., Müller, J.F., Clémer, K., Wang, P., De Mazière, M., Fayt, C., Gielen, C., Hermans, C., Ma, J.Z., Pinardi, G., Stavrakou, T., Vlemmix, T., Van Roozendael, M., 2014. Four years of ground-based MAX-DOAS observations of HONO and NO_2 in the Beijing area. Atmos. Chem. Phys. 14, 765–781.

Hou, S.Q., Tong, S.R., Ge, M.F., An, J.L., 2016. Comparison of atmospheric nitrous acid during severe haze and clean periods in Beijing, China. Atmos. Environ. 124, 199–206.

Hu, Y.J., Lin, J., Zhang, S.Q., Kong, L.D., Fu, H.B., Chen, J.M., 2015. Identification of the typical metal particles among haze, fog, and clear episodes in the Beijing atmosphere. Sci. Total Environ. 511, 369–380.

Hu, Q.Q., Fu, H.B., Wang, Z.Z., Kong, L.D., Chen, M.D., Chen, J.M., 2016. The variation of characteristics of individual particles during the haze evolution in the urban shanghai atmosphere. Atmos. Res. 181, 95–105.
Huang, R.J., Zhang, Y.L., Bozzetti, Carlo, 2014. High secondary aerosol contribution to particulate pollution during haze events in China. Nature 514 (7521), 218–222.
Huang, R.J., Yang, L., Cao, J.J., Wang, Q.Y., Tie, X.X., Ho, Kin-Fai, Shen, Z.X., Zhang, R.J., Li, G.H., Zhu, C.S., Zhang, N.N., Dai, W.T., Zhou, J.M., Liu, S.X., Chen, Y., Chen, J., O'Dowd, Colin D., 2017. Concentration and sources of atmospheric nitrous acid (HONO) at an urban site in Western China. Sci. Total Environ. 593-594, 165–172.
Janhäll, S., Andreae, M.O., Pöschl, U., 2010. Biomass burning aerosol emissions from vegetation fires: particle number and mass emission factors and size distributions. Atmos. Chem. Phys. 10:1427–1439. https://doi.org/10.5194/acp-10-1427-2010.
Kanaya, Y., Cao, R., Akimoto, H., Fukuda, M., Komazaki, Y., Yokouchi, Y., Koike, M., Tanimoto, H., Takegawa, N., Kondo, Y., 2007. Urban photochemistry in central Tokyo: 1. Observed and modeled OH and HO_2 radical concentrations during the winter and summer of 2004. J. Geophys. Res. 112, D21312.
Kim, K.W., Kim, Y.J., Bang, S.Y., 2008. Summer time haze characteristics of the urban atmosphere of Gwangju and the rural atmosphere of Anmyon, Korea. Environ. Monit. Assess. 141 (1–3), 189–199.
Kleffmann, J., Becker, K.H., Lackhoff, M., Wiesen, P., 1999. Heterogeneous conversion of NO_2 on carbonaceous surfaces. Phys. Chem. Chem. Phys. 1 (24), 5443–5450.
Kleffmann, J., Heland, J., Kurtenbach, R., Lörzer, J.C., Wiesen, P., 2002. A new instrument (LOPAP) for the detection of nitrous acid (HONO). Environ. Sci. Pollut. Res. 9, 48–54.
Kleffmann, J., Gavriloaiei, T., Hofzumahaus, A., Holland, F., Koppmann, R., Rupp, L., Schlosser, E., Siese, M., Wahner, A., 2005. Daytime formation of nitrous acid: a major source of OH radicals in a forest. Geophys. Res. Lett. 32, L05818. https://doi.org/10.1029/2005GL022524.
Krueger, B.J., Grassian, V.H., Laskin, A., Cowin, J.P., 2003. The transformation of solid atmospheric particles into liquid droplets through heterogeneous chemistry: laboratory insights into the processing of calcium containing mineral dust aerosol in the troposphere. Geophys. Res. Lett. 30 (3):1148. https://doi.org/10.1029/2002gl016563.
Krueger, B.J., Grassian, V.H., Cowin, J.P., Laskin, A., 2004. Heterogeneous chemistry of individual mineral dust particles from different dust source regions: the importance of particle mineralogy. Atmos. Environ. 38, 6253–6261.
Kurtenbach, R., Becker, K.H., Gomes, J.A.G., Kleffmann, J., Lorzer, J.C., Spittler, M., Wiesen, P., Ackermann, R., Geyer, A., Platt, U., 2001. Investigations of emissions and heterogeneous formation of HONO in a road traffic tunnel. Atmos. Environ. 35, 3385–3394.
Lei, M., Xue, D., Li, C.F., Yin, J.Y., 2013. Study on AOD of Shanghai based on MODIS data. Geo Spa. Info. Technol. 36 (10), 40–43.
Lelieveld, J., Gromov, S., Pozzer, A., Taraborrelli, D., 2016. Global tropospheric hydroxyl distribution, budget and reactivity. Atmos. Chem. Phys. 16 (19), 12477–12493.
Li, W.J., Shao, L.Y., 2009. Transmission electron microscopy study of aerosol particles from the brown hazes in northern China. J. Geophys. Res. 114, D09302. https://doi.org/10.1029/2008JD011285.
Li, Y., An, Y., Min, M., Zhang, W., Wang, F., Xie, P., 2011. Impacts of HONO sources on the air quality in Beijing, Tianjin and Hebei Province of China. Atmos. Environ. 45 (27), 4735–4744.
Li, X., Brauers, T., Haseler, R., Bohn, B., Fuchs, H., Hofzumahaus, A., Holland, F., Lou, S., Lu, K.D., Rohrer, F., Hu, M., Zeng, L.M., Zhang, Y.H., Garland, R.M., Su, H., Nowak, A., Wiedensohler, A., Takegawa, N., Shao, M., Wahner, A., 2012. Exploring the atmospheric chemistry of nitrous acid (HONO) at a rural site in southern China. Atmos. Chem. Phys. 12, 1497–1513.
Li, W.J., Wang, Y., Jeffrey, L., Collett, J., Chen, J.M., Zhang, X.Y., Wang, Z.F., Wang, W.X., 2013. Microscopic evaluation of trace metals in cloud droplets in an acid precipitation region. Environ. Sci. Techno. 47 (9), 4172–4180.
Li, C.L., Hu, Y.J., Chen, J.M., Ma, Z., Ye, X.N., Yang, X., Wang, L., Wang, X.M., Mellouki, Abdelwahid, Mellouki, Abdelwahid, 2015. Physiochemical properties of carbonaceous aerosol from agricultural residue burning: density, volatility, and hygroscopicity. Atmos. Environ. 140, 94–105.
Li, W.J., Shao, L.Y., Zhang, D.Z., Ro, Chul-Un, Hu, M., Bi, X.H., Geng, H., Matsuki, Atsushi, Niu, H.Y., Chen, J.M., 2016. A review of single aerosol particle studies in the atmosphere of East Asia: morphology, mixing state, source, and heterogeneous reactions. J. Clean. Prod. 112, 1330–1349.
Liu, Z., Wang, Y.H., Costabile, Francesca, Amoroso, Antonio, Zhao, C., Greg Huey, L., Stickel, Robert, Liao, J., Zhu, T., 2014. Evidence of aerosols as a media for rapid daytime HONO production over China. Environ. Sci. Technol. 48, 14386–14391.
Lu, K.D., Rohrer, F., Holland, F., Fuchs, H., Bohn, B., Brauers, T., Chang, C.C., Haeseler, R., Hu, M., Kita, K., Kondo, Y., Li, X., Lou, S.R., Nehr, S., Shao, M., Zeng, L.M., Wahner, A., Zhang, Y.H., Hofzumahaus, A., 2012. Observation and modeling of OH and HO_2 concentrations in the Pearl River Delta 2006: a missing OH source in a VOC rich atmosphere. Atmos. Chem. Phys. 12, 1541–1569.
Lu, K.D., Hofzumahaus, A., Holland, F., Bohn, B., Brauers, T., Fuchs, H., Hu, M., Häseler, R., Kita, K., Kondo, Y., Li, X., Lou, S.R., Oebel, A., Shao, M., Zeng, L.M., Wahner, A., Zhu, T., Zhang, Y.H., Rohrer, F., 2013. Missing OH source in a suburban environment near Beijing: observed and modelled OH and HO_2 concentrations in summer 2006. Atmos. Chem. Phys. 13 (2), 1057–1080.
Lv, R., Yu, X.N., Jia, H.L., Xiao, S.H., 2017. Aerosol optical properties and direct radiative forcing at Taihu. Appl. Opt. 56 (25). https://doi.org/10.1364/AO.56.007002.
Nie, W., Ding, A.J., Xie, Y.N., Xu, Z., Mao, H., Kerminen, V.M., Zheng, L.F., Qi, X.M., Huang, X., Yang, X.Q., Sun, J.N., Herrmann, E., Petäjä, T., Kulmala, M., Fu, C.B., 2015. Influence of biomass burning plumes on HONO chemistry in eastern China. Atmos. Chem. Phys. 15, 47–1159.
Okada, K., Qin, Y., Kai, K., 2005. Elemental composition and mixing properties of atmospheric mineral particles collected in Hohhot, China. Atmos. Res. 73 (1–2), 45–67.
Park, S.S., Hong, S.B., Jung, Y.G., Lee, J.H., 2004. Measurements of PM_{10} aerosol and gas phase nitrous acid during fall season in a semi-urban atmosphere. Atmos. Environ. 38 (2), 293–304.
Pathak, R.K., Wu, W.S., Wang, T., 2009. Summertime $PM_{2.5}$ ionic species in four major cities of China: nitrate formation in an ammoniadeficient atmosphere. Atmos. Chem. Phys. 9 (5), 1711–1722.
Qin, M., Xie, P., Su, H., Gu, J., Peng, F., Li, S., Zeng, L., Liu, J., Liu, W., Zhang, Y., 2009. An observational study of the HONO-NO_2 coupling at an urban site in Guangzhou City, South China. Atmos. Environ. 43, 5731–5742.
Rappenglück, B., Lubertino, G., Alvarez, S., Golovko, J., Czader, B., Ackermann, L., 2013. Radical precursors and related species from traffic as observed and modeled at an urban highway junction. J. Air Waste Manage. Assoc. 63, 1270–1286.
Rohrer, F., Berresheim, H., 2006. Strong correlation between levels of tropospheric hydroxyl radicals and solar ultraviolet radiation. Nature 442 (7099), 184–187.
Rubio, Maria, A., Lissi, Eduardo, Villena, Guillermo, 2009. Simultaneous measurements of formaldehyde and nitrous acid in dews and gas phase in the atmosphere of Santiago, Chile. Atmos. Environ. 43 (38), 6106–6109.
Sander, S.P., Friedl, R.R., Golden, D.M., Kurylo, M.J., Moortgat, G.K., Keller-Rudek, H., Wine, P.H., Ravishankara, A.R., Kolb, C.E., Molina, M.J., Finlayson-Pitts, B.J., Huie, R.E., Orkin, V.L., 2006. Chemical Kinetics and Photochemical Data for Use in Atmospheric Studies Evaluation Number 15. 523. Jet Propulsion Laboratory, Pasadena.
Shen, L.J., Zhang, Z.F., 2013. Heterogeneous reactions of NO_2 on the surface of black carbon. Prog. Chem. 25 (1), 28–35.
Shen, X.J., Sun, J.Y., Zhang, X.Y., Zhang, Y.M., Zhang, L., Che, H.C., Ma, Q.L., Yu, X.M., Yue, Y., Zhang, Y.W., 2015. Characterization of submicron aerosols and effect on visibility during a severe haze-fog episode in Yangtze River Delta, China. Atmos. Environ. 120, 307–316.
Sörgel, M., Regelin, E., Bozem, H., Diesch, J.M., Drewnick, F., Fischer, H., Harder, H., Held, A., Hosaynali-Beygi, Z., Martinez, M., Zetzsch, C., 2011. Quantification of the unknown HONO daytime source and its relation to NO_2. Atmos. Chem. Phys. 11, 10433–10447.
Spataro, F., Ianniello, A., Esposito, G., Allegrini, I., Zhu, T., Hu, M., 2013. Occurrence of atmospheric nitrous acid in the urban area of Beijing (China). Sci. Total Environ. 447, 210–224.
Spindler, G., Hesper, J., Bruggemann, E., Dubois, R., Muller, Th., Herrmann, H., 2003. Wet annular denuder measurements of nitrous acid: laboratory study of the artefact reaction of NO_2 with S(IV) in aqueous solutions and comparison with field measurements. Atmos. Environ. 37, 2643–2662.
Stemmler, K., Ammann, M., Donders, C., Kleffmann, J., George, C., 2006. Photosensitized reduction of nitrogen dioxide on humic acid as a source of nitrous acid. Nature 440, 195–198.
Stutz, J., Alicke, B., Ackermann, R., Geyer, A., Wang, S., White, A.B., 2004. Relative humidity dependence of HONO chemistry in urban areas. J. Geophys. Res. 109, D03307. https://doi.org/10.1029/2003JD004135.
Su, H., Cheng, Y.F., Shao, M., Gao, D.F., Yu, Z.Y., Zeng, L.M., Slanina, J., Zhang, Y.H., Wiedensohler, A., 2008. Nitrous acid (HONO) and its daytime sources at a rural site during the 2004 PRIDE-PRD experiment in China. J. Geophys. Res. Atmos. 113 (D14312).
Sullivan, R.C., Guazzotti, S.A., Sodeman, D.A., Prather, K.A., 2007. Direct observations of the atmospheric processing of Asian mineral dust. Atmos. Chem. Phys. 7, 1213–1236.
Sun, Y.L., Zhang, Q., Anastasio, C., Sun, J., 2010. Insights into secondary organic aerosol formed via aqueous-phase reactions of phenolic compounds based on high resolution mass spectrometry. Atmos. Chem. Phys. 10:4809–4822. https://doi.org/10.5194/acp-10-4809-2010.
Taketani, F., Kanaya, Y., Pochanart, P., Liu, Y., Li, J., Okuzawa, K., Kawamura, K., Wang, Z., Akimoto, H., 2012. Measurement of overall uptake coefficients for HO_2 radicals by aerosol particles sampled from ambient air at Mts. Tai and Mang (China). Atmos. Chem. Phys. 12 (24), 11907–11916.
Tang, Y., Huang, Y.L., Li, L., Chen, H., Chen, J.M., Yang, X., Gao, S., Gross, Deborah S., 2014. Characterization of aerosol optical properties, chemical composition and mixing states in the winter season in Shanghai, China. J. Environ. Sci. 26, 2412–2422.
TenBrink, H.M., Veefkind, J.P., Waijersljpelaan, A., VanderHage, J.C., 1996. Aerosol light scattering in the Netherlands. Atmos. Environ. 30 (24), 4251–4261.
Tong, S.R., Hou, S.Q., Zhang, Y., Chu, B.W., Liu, Y.C., He, H., Zhao, P.S., Ge, M.F., 2015. Comparisons of measured nitrous acid (HONO) concentrations in a pollution period at urban and suburban Beijing, in autumn of 2014. SCIENCE CHINA Chem. 58 (9), 1393–1402.
Twohy, C.H., Anderson, J.R., 2008. Droplet nuclei in non-precipitating clouds: composition and size matter. Environ. Res. Lett. 3, 045002.
Villena, G., Wiesen, P., Cantrell, C.A., Flocke, F., Fried, A., Hall, S.R., 2011. Nitrous acid (HONO) during polar spring in Barrow, Alaska: a net source of OH radicals? J. Geophys. Res. Atmos. 116, D00R07.
Wang, S.H., Ackermann, Ralf, Chester Spicer, W., Jerome Fast, D., Schmeling, Martina, Stutz, Jochen, 2003. Atmospheric observations of enhanced NO_2-HONO conversion on mineral dust particles. Geophys. Res. Lett. 30 (11):1595. https://doi.org/10.1029/2003GL017014.
Wang, S., Zhou, R., Zhao, H., Wang, Z., Chen, L., Zhou, B., 2013. Long-term observation of atmospheric nitrous acid (HONO) and its implication to local NO_2 levels in Shanghai, China. Atmos. Environ. 77, 718–724.
Wang, L.W., Wen, L., Xu, C.H., Chen, J.M., Wang, X.F., Yang, L.X., Wang, W.X., Yang, X., Sui, X., Yao, L., Zhang, Q.Z., 2015. HONO and its potential source particulate nitrite at an urban site in North China during the cold season. Sci. Total Environ. 538, 93–101.
Wang, J.Q., Zhang, X.S., Guo, J., Wang, Z.W., Zhang, M.G., 2017. Observation of nitrous acid (HONO) in Beijing, China: seasonal variation, nocturnal formation and daytime budget. Sci. Total Environ. 587-588, 350–359.

Wojtal, P., Halla, J.D., McLaren, R., 2011. Pseudo steady states of HONO measured in the nocturnal marine boundary layer: a conceptual model for HONO formation on aqueous surfaces. Atmos. Chem. Phys. 11, 3243–3261.

Xu, J.W., Tao, J., Zhang, R.J., Cheng, T.T., Leng, C.P., Chen, J.M., Huang, G.H., Li, X., Zhu, Z.Q., 2012. Measurements of surface aerosol optical properties in winter of Shanghai. Atmos. Res. 109-110, 25–35.

Xu, Z., Wang, T., Wu, J.Q., Xue, L.K., Chan, James, Zha, Q.Z., Zhou, S.Z., Louie, Peter K.K., Luk, Connie W.Y., 2015. Nitrous acid (HONO) in a polluted subtropical atmosphere: seasonal variability, direct vehicle emissions and heterogeneous production at ground surface. Atmos. Environ. 106, 100–109.

Ye, B., Ji, X., Yang, H., Yao, X., Chan, C.K., Cadle, S.H., 2003. Concentration and chemical composition of $PM_{2.5}$, in Shanghai for a 1-year period. Atmos. Environ. 37 (4), 499–510.

You, Y., Renbaum-Wolff, L., Carreras-Sospedra, M., Hanna, S.J., Hiranuma, N., Kamal, S., Smith, M.L., Zhang, X., Weber, R.J., Shilling, J.E., Dabdub, D., Martin, S.T., Bertram, A. K., 2012. Images reveal that atmospheric particles can undergo liquideliquid phase separations. Proc. Natl. Acad. Sci. U.S.A. 109 (33), 13188–13193.

Yu, Y., Galle, B., Panday, A., Hodson, E., Prinn, R., Wang, S., 2009. Observations of high rates of NO_2-HONO conversion in the nocturnal atmospheric boundary layer in Kathmandu, Nepal. Atmos. Chem. Phys. 9:6401–6415. https://doi.org/10.5194/acp-9-6401-2009.

Zaizen, Y., Naoe, H., Takahashi, H., Okada, K., 2014. Modification of Asian-dust particles transported by different routes -a case study. Atmos. Environ. 97, 435–446.

Zellweger, C., Ammann, M., Hofer, P., Baltensperger, U., 1999. NO_y speciation with a combined wet effluent diffusion denuder - erosol collector coupled to ion chromatography. Atmos. Environ. 33, 1131–1140.

Zhang, B., Tao, F.M., 2010. Direct homogeneous nucleation of NO_2, H_2O, and NH_3 for the production of ammonium nitrate particles and HONO gas. Chem. Phys. Lett. 489, 143–147.

Zhang, N., Zhou, X., Shepson, P.B., Gao, H., Alaghmand, M., Stirm, B., 2009. Aircraft measurement of HONO vertical profiles over a forested region. Geophys. Res. Lett. 36, L15820. https://doi.org/10.1029/2009GL038999.

Zhang, R., Jing, J., Tao, J., Hsu, S.C., Wang, G., Cao, J., Lee, C.S.L., Zhu, L., Chen, Z., Zhao, Y., Shen, Z., 2013. Chemical characterization and source apportionment of $PM_{2.5}$ in Beijing: seasonal perspective. Atmos. Chem. Phys. 13:7053–7074. https://doi.org/10.5194/acp-13-7053-2013.

Zhou, X., He, Y., Huang, G., Thornberry, T.D., Carroll, M.A., Bertman, S.B., 2002. Photochemical production of nitrous acid on glass sample manifold surface. Geophys. Res. Lett. 29, 1681. https://doi.org/10.1029/2002gl015080.

Zhou, X., Gao, H., He, Y., Huang, G., Bertman, S.B., Civerolo, K., Schwab, J., 2003. Nitric acid photolysis on surfaces in low-NO_x environments: significant atmospheric implications. Geophys. Res. Lett. 30:2217. https://doi.org/10.1029/2003gl018620.

Zhou, X., et al., 2011. Nitric acid photolysis on forest canopy surface as a source for tropospheric nitrous acid. Nat. Geosci. 4:440–443. https://doi.org/10.1038/ngeo1164.

Zhou, Y., Rosen, E.P., Zhang, H., Rattanavaraha, W., Wang, W., Kamens, R.M., 2013. SO_2 oxidation and nucleation studies at near-atmospheric conditions in outdoor smog chamber. Environ. Chem. 10, 210–220.

Zhou, Li, Wang, W.G., Hou, S.Q., Tong, S.R., Ge, M.F., 2015. Heterogeneous uptake of nitrogen dioxide on Chinese mineral dust. J. Environ. Sci. 38, 110–118.

Ziemba, Luke D., Dibb, Jack E., Griffin, Robert J., 2010. Heterogeneous conversion of nitric acid to nitrous acid on the surface of primary organic aerosol in an urban atmosphere. Atmos. Environ. 44 (33), 4081–4089.